Electrostatics-Driven Hierarchical Buckling of Charged Flexible Ribbons

Zhenwei Yao[1,*] and Monica Olvera de la Cruz[2]
[1]Department of Materials Science and Engineering, Northwestern University, Evanston, Illinois 60208-3108, USA and Department of Physics and Astronomy, and Institute of Natural Sciences, Shanghai Jiao Tong University, Shanghai 200240, China
[2]Departments of Materials Science and Engineering, Chemistry, Chemical and Biological Engineering, and Physics, Northwestern University, Evanston, Illinois 60208-3108, USA
(Received 25 January 2016; published 4 April 2016)

We investigate the rich morphologies of an electrically charged flexible ribbon, which is a prototype for many beltlike structures in biology and nanomaterials. Long-range electrostatic repulsion is found to govern the hierarchical buckling of the ribbon from its initially flat shape to its undulated and out-of-plane twisted conformations. In this process, the screening length is the key controlling parameter, suggesting that a convenient way to manipulate the ribbon morphology is simply to change the salt concentration. We find that these shapes originate from the geometric effect of the electrostatic interaction, which fundamentally changes the metric over the ribbon surface. We also identify the basic modes by which the ribbon reshapes itself in order to lower the energy. The geometric effect of the physical interaction revealed in this Letter has implications for the shape design of extensive ribbonlike materials in nano- and biomaterials.

DOI: 10.1103/PhysRevLett.116.148101

An elongated thin ribbon is an ideal model system for representing and understanding a variety of two-dimensional structures in biology [1–3] and nanomaterials [4,5]. Thin ribbons can develop rich morphologies; for example, helical and twisted ribbons constitute the basis for realizing several biological functions [6–8] and designing new structures in nanotechnology [4,5,9]. Several pathways have been proposed to generate various ribbon morphologies, including compressive and tensile loads [10–13] and embedded liquid-crystal orders [2,14]. In recent experiments, the electrostatically driven twist of charged ribbonlike amyloid fibrils has been directly observed in electrolyte solutions [15]. This result distinguishes ribbons from generic spatially extended membranes in terms of their electrostatic response—electrostatics tends to rigidify the membranes and suppress the out-of-plane fluctuations [16]—and it opens the possibility of using electrostatics to manipulate morphologies of ribbonlike objects. Scaling arguments have been proposed to analyze the electrostatically driven morphological transformation of straight and twisted ribbons [15]. The larger shape space of candidate ground states of charged ribbons has not yet been fully explored. In addition, a thorough understanding of how long-range electrostatic potentials deform a charged ribbon is lacking.

To address these fundamental problems, where the challenge results mainly from the coupling of the long-range interactions and ribbon shapes, we resort to numerical simulations in combination with analytical geometric analysis to study the candidate ground states of electrically charged ribbons. We focus on flexible ribbons to highlight the role of electrostatic forces in shaping the low-energy conformations. The bending rigidity κ of a thin elastic sheet can be regarded as vanishingly small according to its power-law dependence on the thickness. Our simulations reveal a variety of low-energy shapes of charged ribbons that can be classified into two types: undulated and twisted conformations. The hierarchical buckling of the ribbon from its initially flat shape to its undulated and then to its out-of-plane twisted conformations is critically controlled by the screening length. The geometric analysis of the stretching patterns over the ribbons indicates that their exhibited rich shapes essentially originate from the electrostatics-driven differentials in the stretching rate along the longitudinal lines from the center to the edge of the ribbons, resulting in the change of the Gaussian curvature. Similar geometric mechanisms govern bucklings in botanical growth and shape-programmable materials, which can create an extraordinary zoo of complex shapes [17]. Notably, rich morphologies of long leaves can be attributed to the differential stretching over the surface caused by the elastic relaxation of biological growth [18]. The geometric effect of long-range electrostatic interactions revealed in this Letter has implications for the shape design of ribbonlike objects in nano- and biomaterials.

The model ribbon is represented by a triangulated surface composed of $N \times M$ vertices, where each vertex is associated with an electric charge $z|e|$. We introduce the Young's modulus K_0 to phenomenologically account for the intermolecular short-range interactions that preserve the structural integrity of the ribbon. In the model, this is represented by neighboring vertices that are connected by bonds of spring constant k_s, which is proportional to

K_0: $K_0 = 4k_s/\sqrt{3}$ for the Poisson ratio $\sigma = 1/3$ [19]. Long-range electrostatic interactions are explicitly included in the model. The effect of the mobile ions in solutions where the ribbons are immersed is taken into consideration by introducing the screening length λ_D. The free energy of the system is therefore

$$F = k_s \sum_{i \in E} (\ell_i - \ell_0)^2 + k_B T l_B z^2 \sum_{i,j \in V} \frac{\exp(-r_{ij}/\lambda_D)}{r_{ij}}.$$

The free energy is defined on the sets of vertices V and edges E. ℓ_i is the bond length of the edge i. The equilibrium lattice spacing ℓ_0 is defined to be unity, serving as the length scale of the system. $l_B = e^2/(4\pi\epsilon_0\epsilon_r k_B T)$ is the Bjerrum length. r_{ij} is the distance between two vertices labeled i and j. The low-energy conformations of the ribbon are controlled by the dimensionless parameter $\Gamma = k_B T l_B z^2/k_s \ell_0^3$ and the screening length λ_D. Note that the presence of counterion condensation may lead to a reduction of the value for Γ, where z is replaced by the smaller effective charge z^*, and an increase of the screening length, which is inversely proportional to the square root of the counterion concentration in solution.

We use the force method to determine the candidate ground states of the ribbon [20,21]. Given an initial conformation of tethered vertices, we simultaneously move all the vertices by $s\hat{w}_k$, where $\hat{w}_k$ is the direction of the movement associated with the vertex k and s is the step size. The unit vector $\hat{w}_k$ is obtained by calculating the force $\vec{F}_k$ on the vertex k by all the other vertices, $\hat{w}_k = \vec{F}_k/\|\vec{F}_k\|$. The system is continuously updated by consecutive sweeps until the energy of the system cannot be reduced any further. In this force-driving protocol, each movement of vertices contributes to the reduction of the energy. This method has been employed to successfully generate low-energy conformations in systems of long-range interacting particles [20,21]. To trigger the out-of-plane deformation, we impose both twisted and cosinelike shapes (see Supplemental Material [22]). It is important to note that the system can be easily trapped in some metastable state in simulations. Consequently, there is high probability that the low-energy conformations found in simulations are not the true ground states. Therefore, we emphasize the modes in which the charged ribbon reshapes itself in order to reach the bottom of the energy basins. From these modes one can capture the characteristic behaviors of the system in approaching the true ground states.

The overall shape of a ribbon can be characterized by the ratio R_{ee}/L, where R_{ee} is the end-to-end distance of the ribbon and L is its contour length. R_{ee}/L is unity for a fully extended straight ribbon, while it is a fraction of a unity for a collapsed conformation. Figure 1 shows the variation of R_{ee}/L with the screening length λ_D for Γ covering a few orders of magnitude. We see that the ribbon is in the collapsed states over a wide range of the screening length $\lambda_D/\ell_0 \in [1, 20]$. Here, without introducing any thermal fluctuation, the appearance of the collapsed states seems intriguing considering that electrostatic repulsion always tends to stretch charged objects to their full extension. The ground state of a charged flexible chain is simply a straight line. To avoid any artifacts arising in simulations, we explicitly compare the energies of these collapsed shapes with their flattened counterparts, which are obtained by flattening the initial shapes. It is found that these collapsed shapes indeed have lower energy.

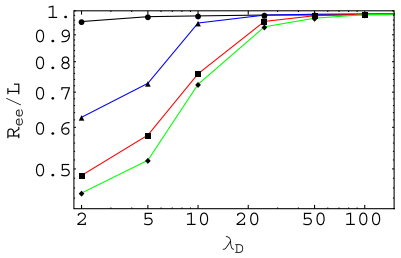

FIG. 1. The ratio of the end-to-end distance R_{ee} of a ribbon to its contour length L vs the screening length λ_D measured in units of the equilibrium bond length ℓ_0. $\Gamma = 1$ (black line, circles), 100 (blue line, triangles), 2500 (red line, squares), and 10 000 (green line, diamonds). The triangulated ribbon is composed of 50×6 vertices.

To understand how the electrostatic repulsion drives the collapse of the ribbon while its generic role is to extend a charged object, we plot the low-energy conformations at several screening lengths in Fig. 2. A close look at the collapsed shapes in Figs. 2(a) and 2(b) shows an important feature that is closely related to the long-range electrostatic interaction. Specifically, in addition to the longitudinal bending, the ribbon is also transversely buckled. The combination of these two bendings gives rise to a positive Gaussian curvature, which is the product of the two principal curvatures κ_1 and κ_2 at a point on a smooth surface [23]. The shape of the central protrusion in Fig. 2(a), a typical shape element in undulated conformations, is similar to that of the outer edge of a car tire; the Gaussian curvature of both objects is positive. All the undulated ribbons found in simulations can break into a chain of these positively curved tirelike shapes. The robustness of these undulated structures is substantiated in extensive simulations, where both the wavelength and the type of the initial shape are varied.

The origin of these elementary tirelike shapes can be attributed to the geometric effect of the long-range electrostatic interaction. We plot the distribution of the bond length along the longitudinal curves on the ribbon in Figs. 2(e)–2(h), where the colored curves correspond to the longitudinal curves of the same color in Figs. 2(a)–2(d), respectively. It clearly shows that the bonds are *inhomogeneously* stretched by the electrostatic repulsion. The central regions of the ribbons in Figs. 2(a) and 2(b) are more

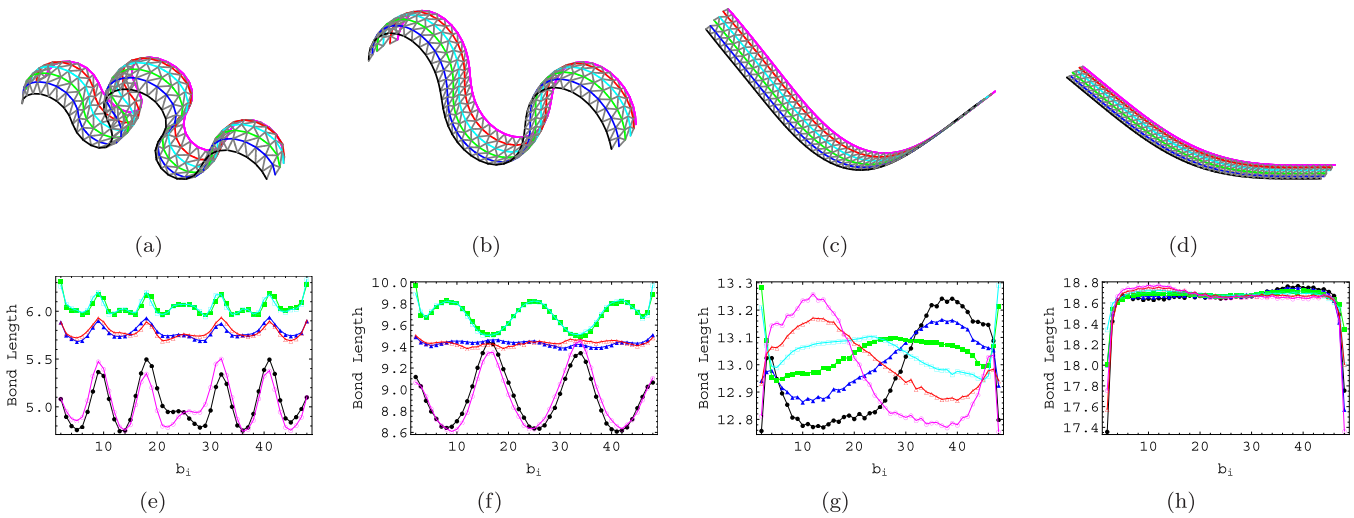

FIG. 2. The low-energy conformations of the charged flexible ribbon and the corresponding distribution of the bond length along the longitudinal curves on the ribbon. $\lambda_D = 2$, 5, 10, 25 from (a) to (d) and from (e) to (h), respectively. b_i represents the bond between vertices i and $i+1$, both of which are located on the same longitudinal curve (the same-colored curve). The triangulated ribbon is composed of 50×6 vertices, and $\Gamma = 10^4$.

stretched than the edges, as seen in Figs. 2(e) and 2(f). The distribution of the longitudinal stretching is almost symmetric about the central longitudinal line on the ribbon. The differentials in the stretching rate along the longitudinal lines from the center to the edge of the ribbon are caused by the variation of the electrostatic forces on the spring bonds along different longitudinal lines. In the regime of short screening length, the particles at the ends of a spring bond along the central longitudinal line are subject to larger electrostatic forces from more charged neighboring particles in comparison to that along the longitudinal edges. We invoke Gauss's theorema egregium to illustrate why this kind of inhomogeneous stretching can lead to the buckling of the ribbon to a positively curved tirelike shape. Gauss's theorem states that the Gaussian curvature depends solely on the metric of the surface instead of its shape. It is quantitatively expressed by the equation [23]

$$K_G = -\frac{1}{\sqrt{g}}\left[\partial_u\left(\frac{1}{\sqrt{g_{uu}}}\partial_u\sqrt{g_{vv}}\right) + \partial_v\left(\frac{1}{\sqrt{g_{vv}}}\partial_v\sqrt{g_{uu}}\right)\right],$$

which gives the Gaussian curvature distribution over the surface $\vec{x}(u,v)$ whose metric is characterized by $ds^2 = g_{uu}du^2 + g_{vv}dv^2$ with $g_{uv} = g_{vu} = 0$.

The inhomogeneous stretching over the ribbon surface can be described by the metric $ds^2 = [1+h(y)]^2dx^2 + dy^2$, where the x and y axes are along the longitudinal and transverse directions, respectively. For simplicity, the transversal stretching is not taken into consideration. The information of the stretching is encoded in $h(y)$, which is a concave function in its domain $y \in [-b/2, b/2]$, with b being the width of the ribbon. It is derived that $K_G = -[h''(y)]/[1+h(y)] > 0$, where the inequality is due to the concavity of $h(y)$. The positive Gaussian curvature, which results from the stretching along the central longitudinal lines being larger than that along the longitudinal edges, can also be seen from the fundamental definition of the Gaussian curvature. Positive Gaussian curvature will ensue when the inside stretches more than the outside. As an example, take a spherical cap: it has a smaller circumference than one expects on a planar disk. Therefore, the appearance of the buckled tirelike shapes that are responsible for the collapse of the ribbon can be traced down to the electrostatically driven inhomogeneous stretching that changes the metric of the ribbon surface. In the Supplemental Material [22], we present another case of the electrostatically driven buckling of a single hexagon and discuss the geometric effect of the electrostatic interaction in that simpler system [22]. Note that the uniform transverse buckling along bilayer ribbons has been studied by de Gennes as a method to form tubes [24]. Following this spirit, the doubly buckled tirelike shapes might lead to the formation of toroidal objects.

In the regime of sufficiently short screening length, the ribbon prefers an undulated conformation over a wide range of the values for the aspect ratio $\tau = M/N \in [0.01, 0.6]$. When the screening length exceeds some critical value, an undulated long ribbon is numerically observed to be twisted out of the plane. In this process, the stretching pattern over the ribbon changes correspondingly. Figure 2(g) shows that over the two relatively flat portions of the bent ribbon in Fig. 2(c), the same longitudinal curve that is stretched the most in one portion is stretched the least in the other one. We will see that the twisted V-like object demonstrated in Fig. 2(c) is an elementary shape to constitute a long twisted ribbon.

The identified electrostatically driven twist of the ribbon implies the possibility of forming helical structures in sufficiently long ribbons. Figure 3 shows several typical structures found in simulations, including undulated, helical, and irregularly deformed ribbons. In the regime of short screening length, the ribbon is always undulated, and the longitudinal curves in the ribbon almost lie in the plane, as exemplified in Fig. 3(a). The number of waves decreases from ~10 to a fraction of 10 when the screening length increases from unity to about 4 for $\Gamma \in [1, 10^4]$. These waves on the undulated ribbons are the precursors for the helical portions in the twisted ribbons; the wavelength defines the size of the pitch in the perspective helical structure. When the screening length exceeds some critical value, these waves twist to either the left or the right side of the plane where the ribbon lies. A helical ribbon is formed when the twist of all the waves is uniformly towards the same direction. Figures 3(a) and 3(b) show such an undulated-to-twisted transition via the concerted twist of all the waves on the undulated ribbon. While helical structures with an electrostatic origin have been found in confined systems [25,26], here we report the electrostatically driven freestanding helical ribbons.

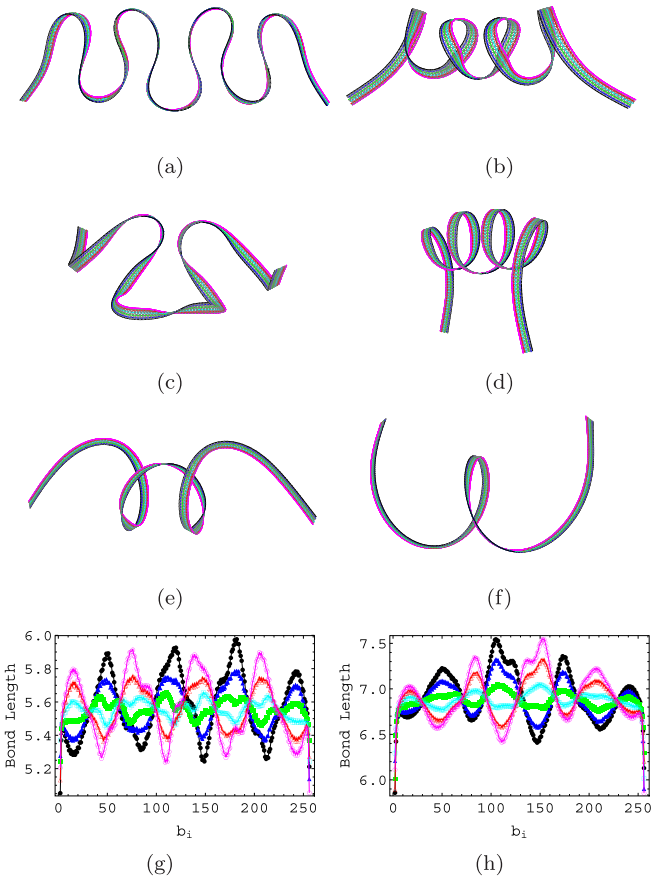

FIG. 3. The originally undulated ribbon (a) is twisted out of the plane with the increase of the screening length. $\lambda_D = 4$, 8, 16, 20, 28, and 50 from (a) to (f). The distributions of the bond length along the longitudinal curves on the ribbons in (b) and (c) are plotted in (g) and (h), respectively. The triangulated ribbon is composed of 258×6 vertices and $\Gamma = 196$.

Figures 3(g) and 3(h) show the distribution of the bond length along the longitudinal curves on the helical ribbon in Fig. 3(b) and the irregularly deformed ribbon in Fig. 3(c), respectively. One striking feature is the periodic and out-of-phase variation of the stretching along the edges of the ribbons, i.e., the black (circle) and pink (empty circle) curves. This indicates that a twisted ribbon can be divided into a number of twisted segments. One such segment, i.e., a twisted V-like shape as in Fig. 2(c), corresponds to a wave in the plot of the bond length distribution. This elementary structure is also widely found among long and irregularly buckled ribbons, as exemplified in Fig. 3(h) for the shape in Fig. 3(c). In extensive simulations of flexible ribbons whose aspect ratio ranges from 0.01 to 0.6, freestanding straight twisted ribbons are not found, although the electrostatic energy of a ribbon can be reduced by twisting along its central axis [15,27]. This suggests that other constraints may be required to stabilize an electrically charged straight twisted ribbon. In addition, helical ribbons with both chiralities are found in simulations, showing that pure electrostatic interactions do not endow the helical structures with a specific chirality.

The phase diagram in the parameter space spanned by Γ and the screen length λ_D is presented in Fig. 4. The curves that represent ribbons of different aspect ratios separate the undulated state (below the curve) and the twisted state (above the curve). The critical values for the screening length lie within a relatively narrow interval. It indicates that the twist of the ribbon is largely triggered by the screening length for $\Gamma \in [1, 10^4]$. In other words, the action range, rather than the strength of the electrostatic

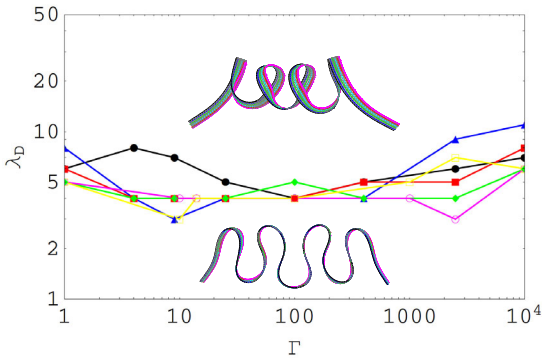

FIG. 4. The phase diagram of the low-energy shapes of the charged ribbon. The curves separate the undulated state (below the curve) and the twisted state (above the curve). For flexible ribbons with vanishing bending rigidity, $M = 6$ and $N = 102$ (black circles), 154 (blue triangles), 206 (red squares), and 258 (green diamonds). The two curves with empty symbols are for ribbons with bending rigidity $\kappa/(K_0\ell_0^2) = 0.1$ (pink empty circles) and 0.01 (yellow empty squares) (see Supplemental Material [22]), with $M = 6$ and $N = 258$.

interaction, matters for the twist of the undulated ribbon. Simulations show that for sufficiently large screening length, typically $\lambda_D \gg 50$ for ribbons with $M = 6$ and $N \in [50, 258]$, the ribbon will ultimately be stretched towards a straight line. This is reasonable, because when λ_D is much larger than the width of the ribbon, the ribbon essentially reduces to a geometric line. We see from Fig. 2(h) that at large screening length the entire ribbon tends to be uniformly and strongly stretched, except its ends which are less stretched because of the reduced electrostatic energy therein. Similar uneven distribution of electrostatic repulsion-driven stretching is also seen in polyelectrolyte chains leading to trumpetlike shapes [28]. In the regime of weak electrostatic interactions or strong stretching rigidity ($\Gamma \lesssim 10^{-2}$), the ribbons are slightly undulated, and no twist deformation is observed. Here, it is important to note that the dimension of width on the ribbon supports the spatially varying stretching and the underlying curvature structure, which are crucial for generating various morphologies. For charged flexible square sheets, simulations show that the out-of-plane deformations occur only in the regime of very short screening length (see Supplemental Material [22]).

In summary, we investigate the rich morphologies exhibited by charged flexible ribbons, and identify the electrostatics-driven hierarchical buckling of the ribbon from its initially flat shape to its undulated and then to its out-of-plane twisted conformations. In this process, the screening length is the key controlling parameter. Extensive data analysis shows that the ribbon shapes originate from the geometric effect of the electrostatic interaction that redefines the metric over the ribbon surface. The geometric effect of the physical interaction revealed in this Letter has implications for the shape design of extensive ribbonlike objects in nano- and biomaterials.

This work was supported as part of the Center for Bio-Inspired Energy Science, an Energy Frontier Research Center funded by the U.S. Department of Energy, Office of Science, Basic Energy Sciences, under Award No. DE-SC0000989-002. Z. Y. acknowledges support from the SJTU startup fund and the award of the Chinese Thousand Talents Program for Distinguished Young Scholars.

*Corresponding author.
zyao@sjtu.edu.cn

[1] D. S. Chung, G. B. Benedek, F. M. Konikoff, and J. M. Donovan, Proc. Natl. Acad. Sci. U.S.A. **90**, 11341 (1993).
[2] R. L. B. Selinger, J. V. Selinger, A. P. Malanoski, and J. M. Schnur, Phys. Rev. Lett. **93**, 158103 (2004).
[3] H. Cui, T. Muraoka, A. G. Cheetham, and S. I. Stupp, Nano Lett. **9**, 945 (2009).
[4] Z. W. Pan, Z. L. Wang *et al.*, Science **291**, 1947 (2001).
[5] X. Li, X. Wang, L. Zhang, S. Lee, and H. Dai, Science **319**, 1229 (2008).
[6] L. C. Palmer, Y. S. Velichko, M. Olvera de la Cruz, and S. I. Stupp, Phil. Trans. R. Soc. A **365**, 1417 (2007).
[7] E. T. Pashuck and S. I. Stupp, J. Am. Chem. Soc. **132**, 8819 (2010).
[8] T. J. Moyer, H. Cui, and S. I. Stupp, J. Phys. Chem. B **117**, 4604 (2013).
[9] C. Vallés, C. Drummond, H. Saadaoui, C. A. Furtado, M. He, O. Roubeau, L. Ortolani, M. Monthioux, and A. Pénicaud, J. Am. Chem. Soc. **130**, 15802 (2008).
[10] A. Green, Proc. R. Soc. A **161**, 197 (1937).
[11] S. Panyukov and Y. Rabin, Europhys. Lett. **57**, 512 (2002).
[12] R. Ghafouri and R. Bruinsma, Phys. Rev. Lett. **94**, 138101 (2005).
[13] J. Chopin and A. Kudrolli, Phys. Rev. Lett. **111**, 174302 (2013).
[14] Y. Sawa, F. Ye, K. Urayama, T. Takigawa, V. Gimenez-Pinto, R. L. Selinger, and J. V. Selinger, Proc. Natl. Acad. Sci. U.S.A. **108**, 6364 (2011).
[15] J. Adamcik and R. Mezzenga, Soft Matter **7**, 5437 (2011).
[16] D. Andelman, Electrostatic properties of membranes: The Poisson-Boltzmann theory, *Handbook of Biological Physics* 1, 603–642 (Elsevier, Amsterdam, 1995).
[17] C. D. Modes and M. Warner, Phys. Rev. E **92**, 010401 (2015).
[18] H. Liang and L. Mahadevan, Proc. Natl. Acad. Sci. U.S.A. **106**, 22049 (2009).
[19] *Statistical Mechanics of Membranes and Surfaces*, 2nd ed., edited by D. Nelson, T. Piran, and S. Weinberg (World Scientific, Singapore, 2004).
[20] E. Bendito, M. J. Bowick, A. Medina, and Z. Yao, Phys. Rev. E **88**, 012405 (2013).
[21] Z. Yao and M. Olvera de la Cruz, Phys. Rev. Lett. **111**, 115503 (2013).
[22] See Supplemental Material at http://link.aps.org/supplemental/10.1103/PhysRevLett.116.148101 for technical details of simulations and more supplementary results about the buckling of a charged square sheet and a single hexagon.
[23] D. Struik, *Lectures on Classical Differential Geometry*, 2nd ed. (Dover, New York, 1988).
[24] P. G. de Gennes, Electrostatic buckling of chiral lipid bilayers, *Comptes rendus de l'Académie des Sciences* 304, 259–263 (Elsevier, Paris, 1987).
[25] K. L. Kohlstedt, F. J. Solis, G. Vernizzi, and M. Olvera de la Cruz, Phys. Rev. Lett. **99**, 030602 (2007).
[26] G. Vernizzi, K. L. Kohlstedt, and M. Olvera de la Cruz, Soft Matter **5**, 736 (2009).
[27] L. Onsager, Ann. N.Y. Acad. Sci. **51**, 627 (1949).
[28] M. Castelnovo, P. Sens, and J.-F. Joanny, Eur. Phys. J. E **1**, 115 (2000).